

Supporting information

Electronic pyroelectricity in a supramolecular assembly of acceptor-donor-acceptor type ambipolar π -system

Pritam Sadhukhan,^{a,†} Sk Kalimuddin,^{b,†} Aritri Pal,^a Tuhin Debnath,^b Swadesh Paul,^a Shubhankar Barman,^a Suhrit Ghosh,^{*a,c} Mintu Mondal,^{*b} and Anuja Datta^{*a,c}

a. School of Applied and Interdisciplinary Sciences

b. School of Physical Sciences

c. Technical Research Centre

Indian Association for the Cultivation of Science, 2A and 2B Raja S. C. Mullick Road, Kolkata, India-700032.

Email: SG psusg2@iacs.res.in MM sspmm4@iacs.res.in AD psuad4@iacs.res.in

† Contributed equally

Table of contents

Title	Page No.
1. Table S1 - Comparison of pyroelectric performance parameters of c with reported soft pyroelectrics	3
2. Table S2 - Comparison of energy harvesting performance of AD ₂ A-based pyroelectric device with reported soft pyroelectrics-based devices	4
3. Table S3. Saturation time-scale	5
4. Figure S1 - Some characterizations of the AD ₂ A material	5
5. Figure S2 - Pyroelectric properties of the AD ₂ A film-based device	6
6. Figure S3 – p vs. ϵ_r of polymer based soft pyroelectric materials	7
7. Figure S4 - Pyroelectric properties of control polymers	8
8. Figure S5 - Pyroelectric current response of the AD ₂ A polymer system upon thermal oscillation at different background temperatures	9
9. Figure S6 - The cyclic changes in temperature of the AD ₂ A pyroelectric generator device and the corresponding first derivative of temperature with time	9
10. Figure S7 - The cyclic changes in temperature of the AD ₂ A pyroelectric generator device and the measured short-circuit current at reversed connection to the measurement system	10
11. Figure S8 - Output stability test of the AD ₂ A pyroelectric generator device	10
12. Figure S9 - The plot of output peak current vs. ΔT obtained from the AD ₂ A pyroelectric generator device.	11
13. Figure S10 - The cyclic changes in temperature of the reference systems C1 and C2 and the measured short-circuit current at forward connection to the measurement system	11
14. Fig. S11- Plot of sample surface temperature vs time corresponding to different light intensities	12
15. Figure S12 - Response time of the AD ₂ A film-based generator device	12
16. Figure S13 - Plot of peak current release with power density of green laser light (532 nm) under different DC bias voltage conditions.	13
17. Figure S14 - Photoresponsivity and detectivity of AD ₂ A film device under weak light power density of 532 nm laser.	13
18. Figure S15 - Behavior of photoresponsivity within the temperature range 300-380 K.	14
19. Supplementary Note - Pyroelectric figure-of-merits (FOMs)	14
20. Supplementary Note - Preparation of films for pyroelectric measurements	15
21. Supplementary Note - Device fabrication for pyroelectric measurements	15
22. Supplementary Note - Photo-pyroelectric response parameters	15
23. Supplementary Note - Pyroelectric energy harvesting by Olsen cycle	15
24. References	16

Table S1: Comparison of pyroelectric performance parameters of AD₂A with reported soft pyroelectrics.

Materials	<i>T</i>	<i>P</i> ($\mu\text{C m}^{-2} \text{K}^{-1}$)	ϵ_r	<i>F_V</i> ($\text{m}^2 \text{C}^{-1}$)	<i>F_D</i> ($10^{-5} \text{pa}^{0.5}$)	References
PVDF	RT	27	12	0.105	0.88	Ref. ^{1,2}
P(VDF/TrFE) 80/20	RT	31	7	0.217	1.40	Ref. ^{3,4}
P(VDF/TrFE) 60/40	RT	51	19.4	0.13	0.838	Ref. ⁵
P(VDF/TrFE) 70/30	RT	33	7.4	0.22	1.36	Ref. ^{4,6}
P(VDF/TrFE) 56/44	RT	52	18	0.148	0.81	Ref. ⁷
P(VDF/TrFE) 50/50	RT	40	18	0.109	0.148	Ref. ⁷
	<i>T_C</i>	142	33	0.04	0.221	
Polyvinyl Fluoride (PVF)	RT	18	5	0.177	0.53	Ref. ^{8,9}
Polyvinyl Chloride (PVC)	RT	1	5	-	-	Ref. ⁸
Polyacrylonitrile (PAN)	RT	1	7.7	-	-	Ref. ⁸
AD₂A	RT	3.5	45.2	0.001	0.08	This work
	<i>T_C</i>	206	79.4	0.11	1.01	

Table S2. Saturation time-scale: Time it takes to reach a certain temperature under different light powers.

S. No	λ (nm)	Intensity (mW/cm ²)	Time (sec)
1	532	146	6.16
2	532	130	3.79
3	532	120	4.76

Table S3: Comparison of energy harvesting performance of AD₂A-based pyroelectric device with reported soft pyroelectrics-based devices.

Materials	T_C ($^{\circ}C$)	T_H ($^{\circ}C$)	E_L (MV/m)	E_H (MV/m)	N_D (J/L/cycle)	P_D (W/L)	Ref.
73/27 P(VDF- TrFE)	23	67	23.0	53.0	30	2.38	Ref. ¹⁰
60/40 P(VDF- TrFE)	25	120	20.0	60.0	900	112.5	Ref. ¹¹
60/40 P(VDF- TrFE)	58	77	4.1	47.2	52	13.3	Ref. ¹²
60/40 P(VDF- TrFE)	50	100	6.23	27.6	165	-	Ref. ¹³
60/40 P(VDF- TrFE)	67	81	20.3	37.9	130	10.7	Ref. ¹⁴
60/40 P(VDF- TrFE)	25	110	20.0	50.0	521	-	Ref. ¹¹

61.3/29.7/9 P(VDF- TrFE- CFE)	0	25	0.0	25.0	50	-	Ref. ¹⁵
56/44 P(VDF- TrFE)	40	100	5	50	-	110	Ref. ¹⁶
AD₂A	27	97	0.35	0.56	1.45	0.097	This work

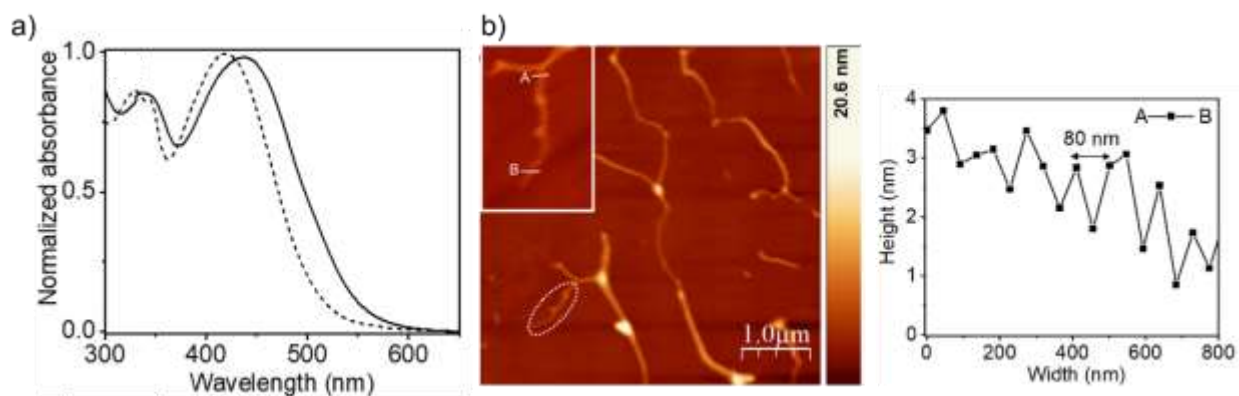


Fig. S1. (a) UV/ Vis spectra of AD₂A in 0.1 mM THF solution (broken lines) and in the film state (solid lines); (b) AFM height image of supramolecular assembly of AD₂A. Sample were prepared by spin-coating an aggregated solution in MCH (0.1 mM) on freshly cut mica. Insets shows enlarged view of a selected fibre (indicated by white circle) with right-handed helicity. Height analysis along A-B in the zoomed image is shown in the right panel which confirms helical nature of the fibres. Adapted with permission from our previously reported paper (*Chem. Sci.*, 2022, **13**, 781).

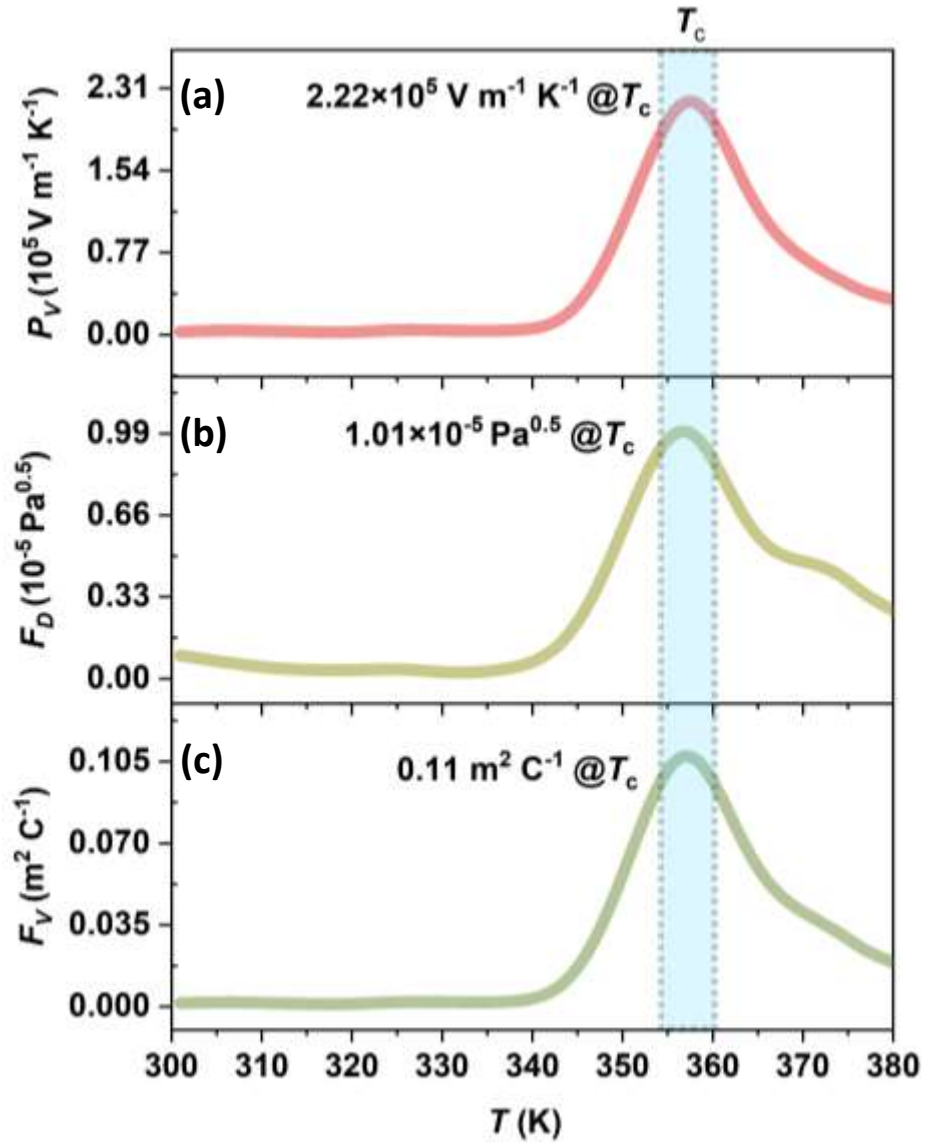


Fig. S2. Pyroelectric properties of the AD₂A film-based device. (a) Pyroelectric voltage coefficient (P_V); (b) FOM of detectivity (F_D); (c) FOM of voltage responsivity (F_V).

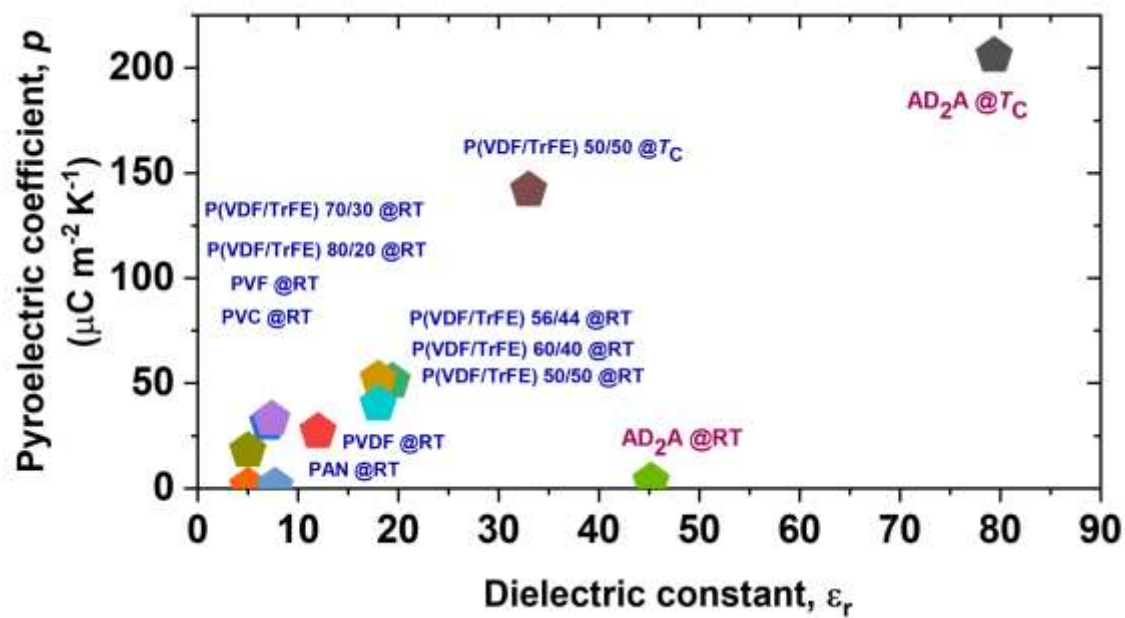


Fig. S3. p vs. ϵ_r of polymer based pyroelectric materials.

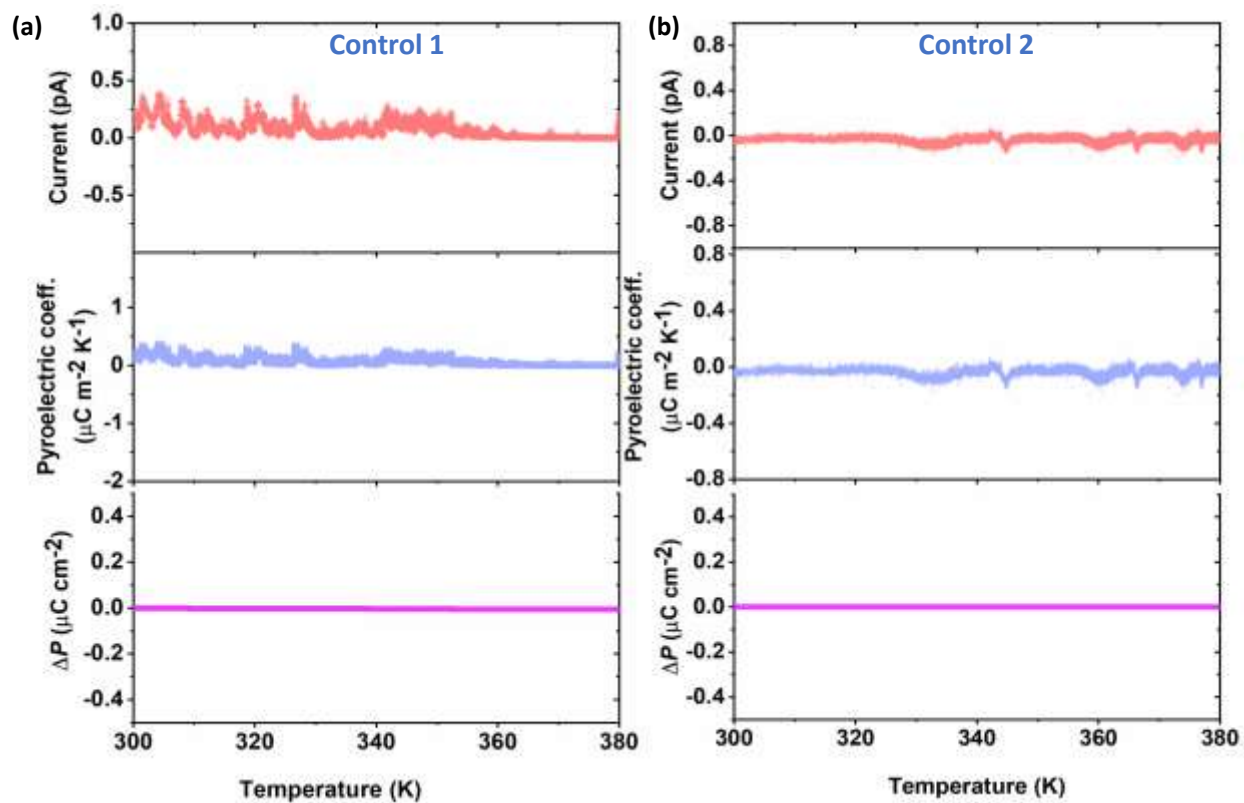


Fig. S4. Pyroelectric properties of control molecules control 1 (a) and control 2 (b).

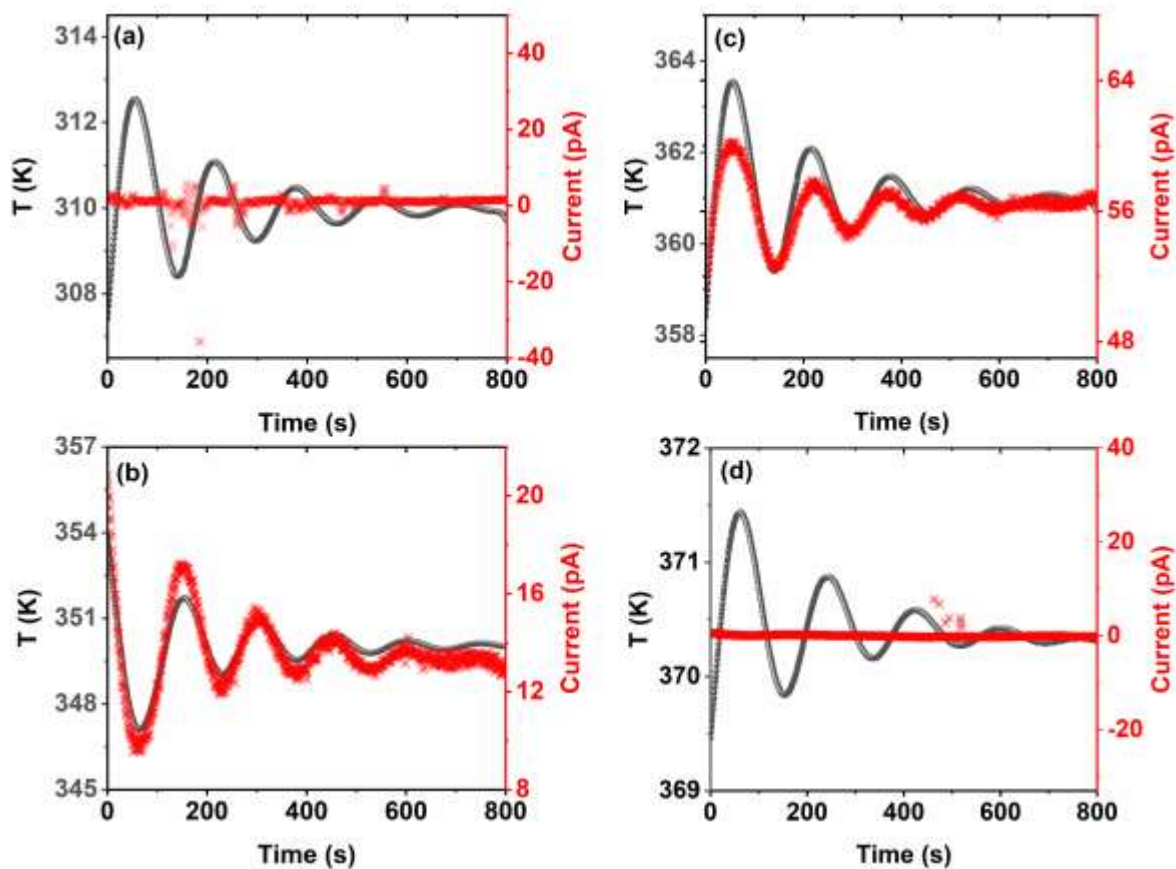


Fig. S5. Pyroelectric current response of the AD₂A system upon thermal oscillation at different background temperatures.

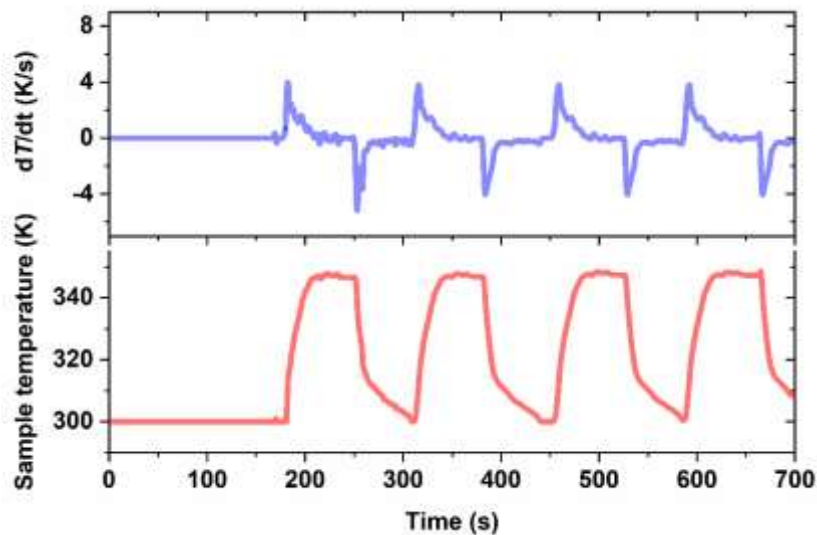


Fig. S6. The cyclic changes in temperature of the AD₂A pyroelectric generator device and the corresponding first derivative of temperature with time.

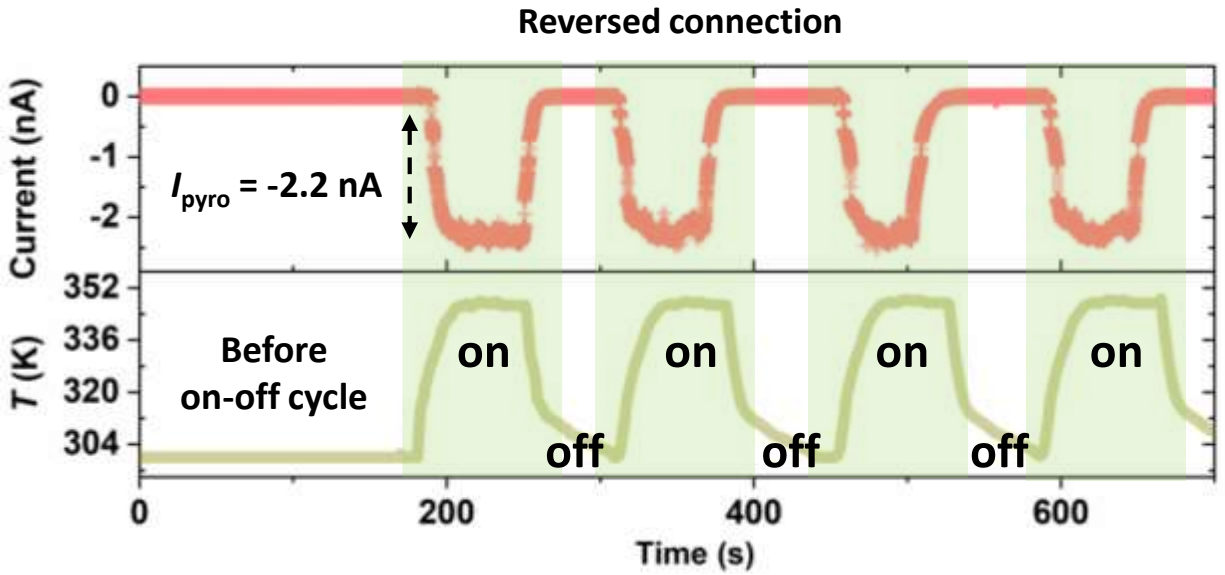


Fig. S7. The cyclic changes in temperature of the AD₂A pyroelectric generator device and the measured short-circuit current at reversed connection to the measurement system.

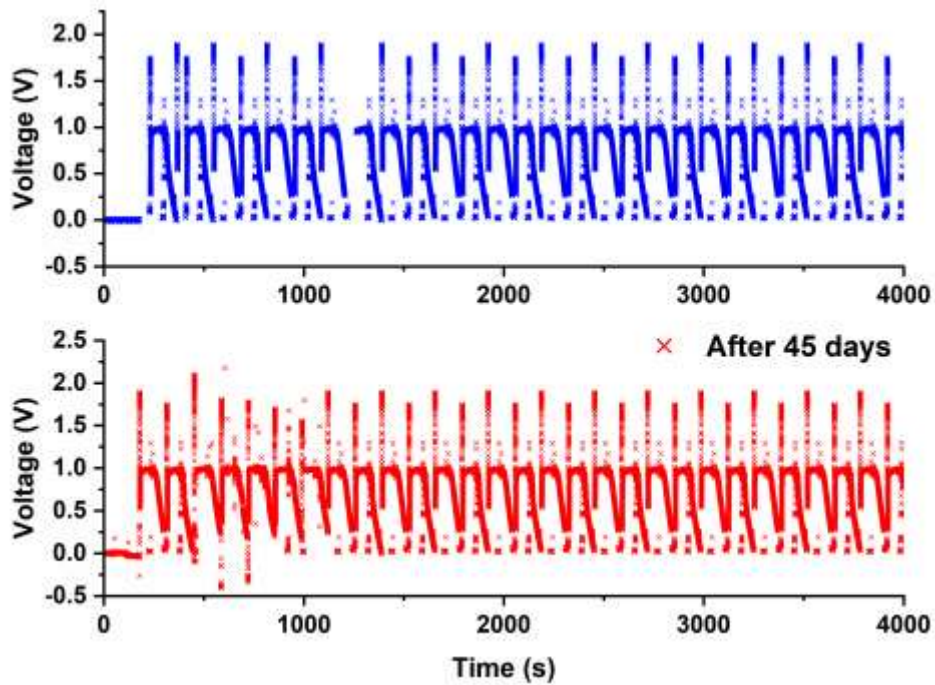


Fig. S8. (a) Output stability test of the AD₂A pyroelectric generator device through cyclic temperature change for over 25 cycles. (b) Output stability test on the same device after 45 days.

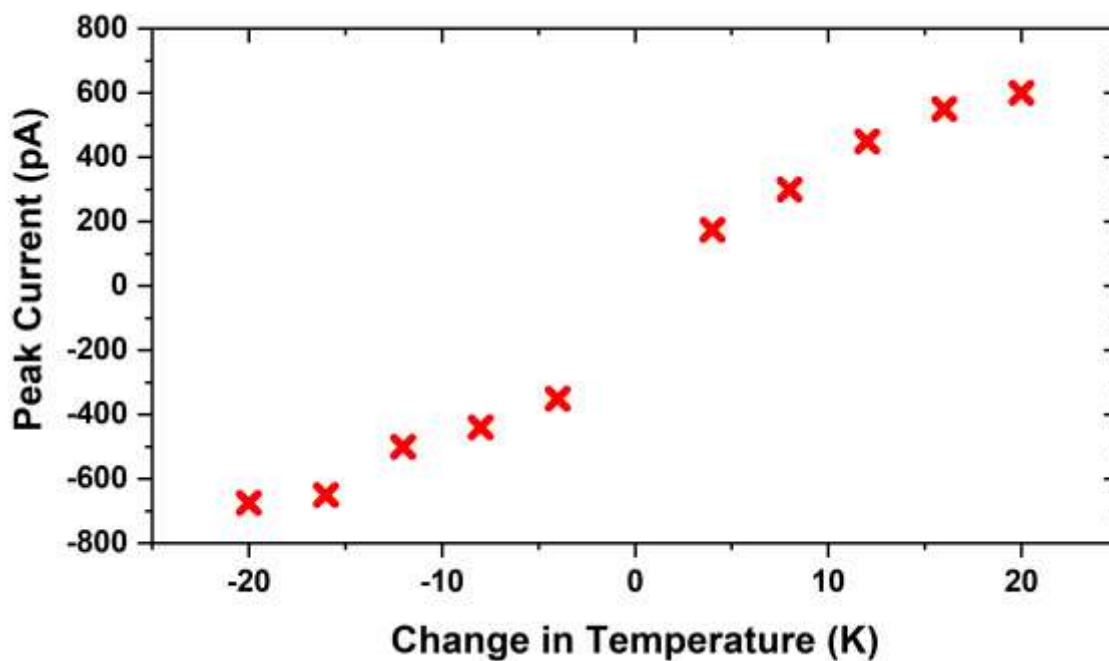


Fig. S9. The plot of output peak current vs. ΔT obtained from the AD₂A pyroelectric generator device.

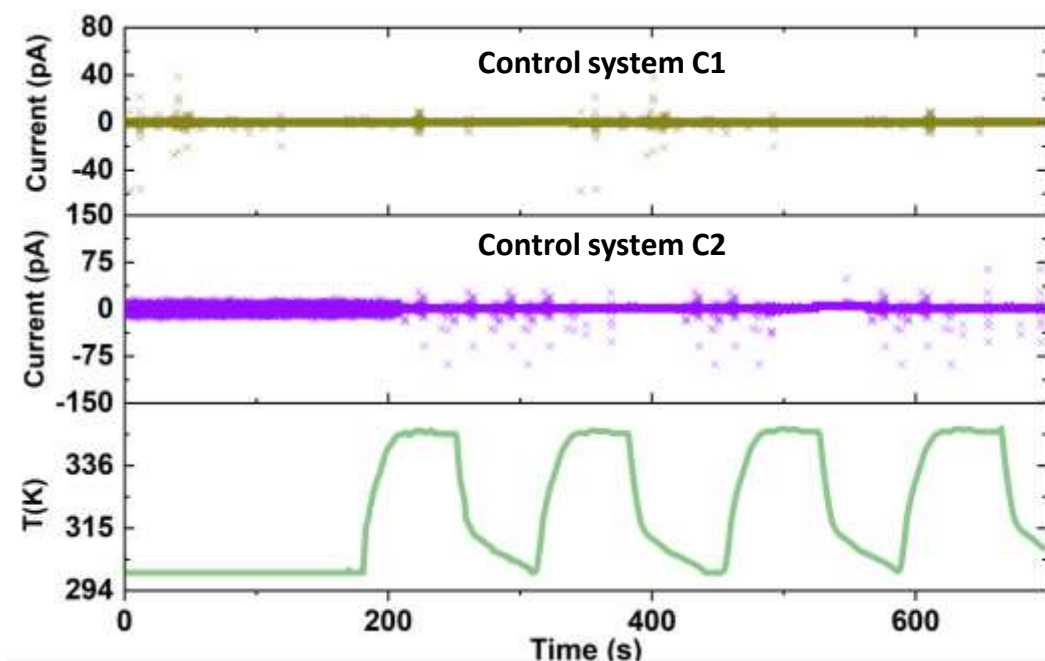


Fig. S10. The cyclic changes in temperature of the reference systems C1 and C2 and the measured short-circuit current at forward connection to the measurement system.

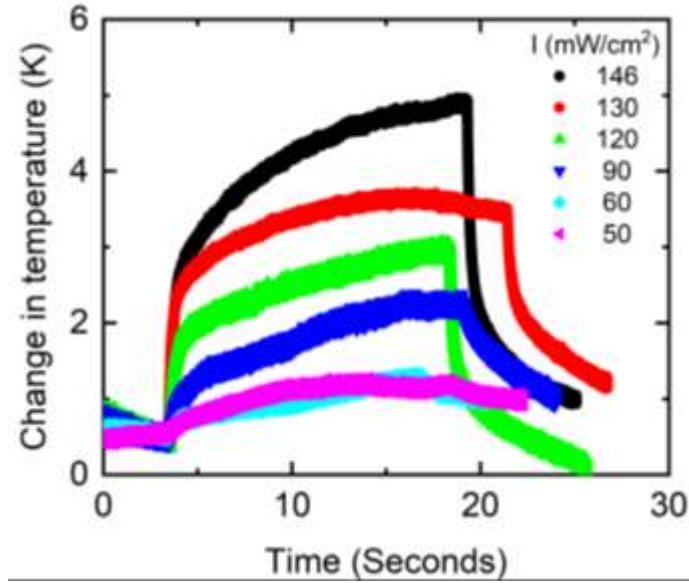


Fig. S11: Plot of sample surface temperature vs time corresponding to different light intensities of 146,130,120,90,60, and 50 mW/cm².

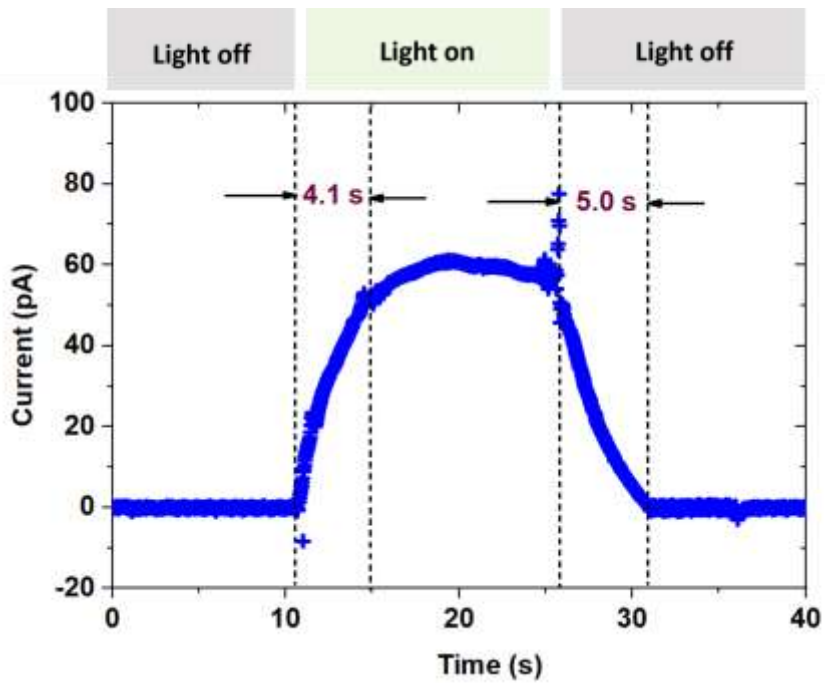


Fig. S12. Response time of the AD₂A film-based generator device.

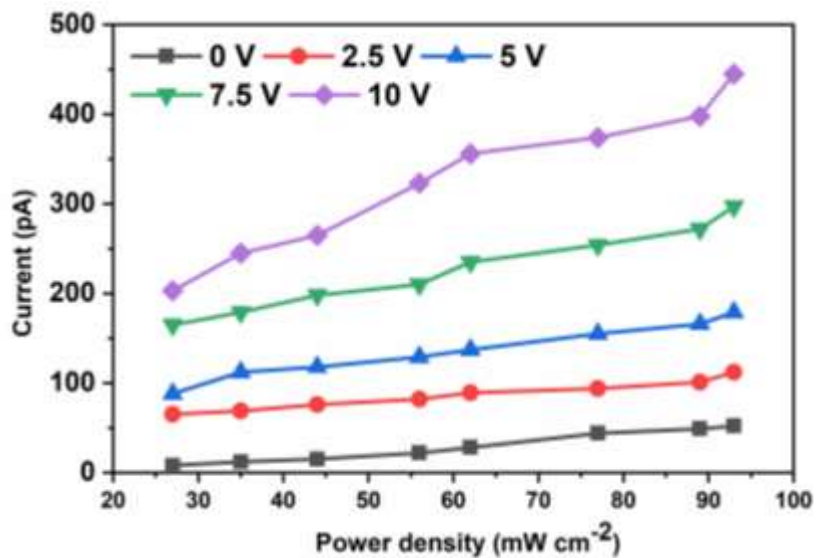


Fig. S13. Plot of peak current release with power density of green laser light under different DC bias voltage conditions.

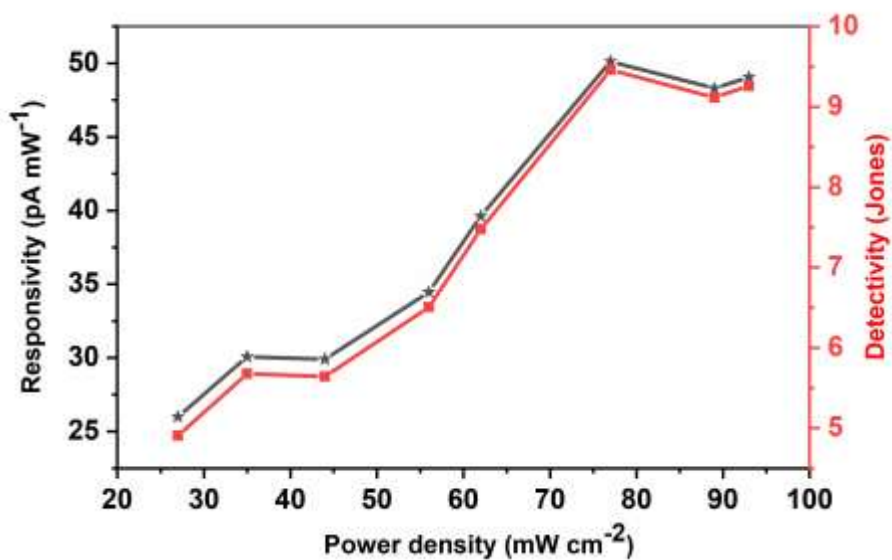


Fig. S14. Photoresponsivity and detectivity of AD₂A film device under weak light power density of green laser.

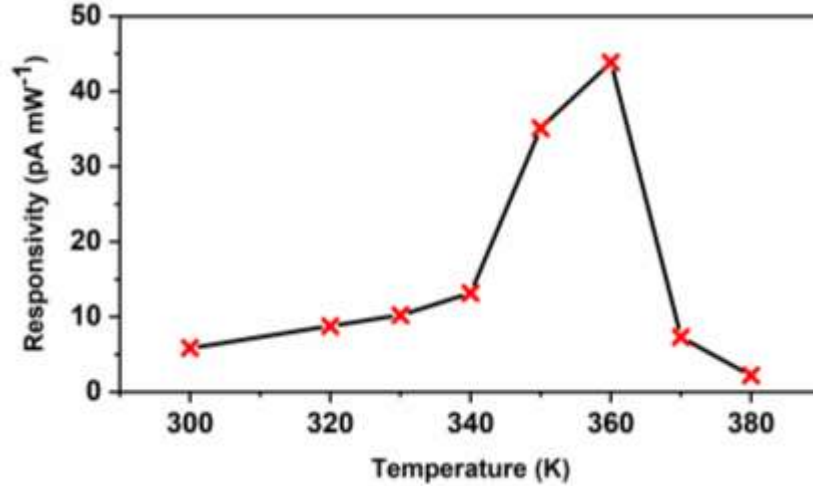


Fig. S15. Behavior of photoresponsivity within the temperature range 300-380 K.

Supplementary Note

Pyroelectric figure-of-merits (FOMs)

For pyroelectric energy harvesting prospects, the figure of merit (FOM) is $F_E = p^2/(\epsilon_0\epsilon_r)$, which represent the amount of electric power converted from a given thermal energy input.¹⁷ Here, p represents pyroelectric current coefficient, ϵ_0 is vacuum permittivity and ϵ_r is relative permittivity.

In case of pyroelectric sensors, the FOMs are voltage responsivity $F_V = p/(\epsilon_0\epsilon_r C_V)$ and detectivity $F_D = p/[C_V(\epsilon_0\epsilon_r \tan\delta)^{0.5}]$, where F_V represents the maximum pyroelectric voltage for a specific energy input, while F_D represents the propensity of detectors to sense weak signals. C_V is volume specific heat and $\tan \delta$ represents dielectric loss.

Experimental details of pyroelectric studies:

Preparation of films for pyroelectric measurements

Using ultrasonication at room temperature (30°C) for 1h, 5.0 mM solutions of AD₂A, C1 or C2 were prepared in spectroscopy grade methylcyclohexane (MCH). 3 x 5 mm ITO coated glass

substrates (Techinstro, India) with a surface resistivity of approximately 5 ohm/sq were cleaned using absolute ethanol and acetone before being air dried at room temperature. The films were made by spin-coating (Apex Ltd., India; spin speed = 250 rpm, acceleration = 5 rpm/sec). Further, the film was allowed to dry for 12 hours under suction. Using a Mitutoyo Micrometer (Model No. 293-240-30), the film's thicknesses were determined to be approximately 60 microns.

Device fabrication for pyroelectric measurements

To create the architecture of a pyroelectric generator device, Ag epoxy (Sigma-Aldrich) electrode was deposited on the top of the film (electrode area = 9.6 mm²). Another silver electrode was deposited on the bottom ITO/glass substrate (Fig. 1). 0.1 mm Cu wires were attached to both the electrodes. The resulting pyroelectric generator was employed for all the electric measurements after being dried under vacuum for 24 hours. To ensure consistent data, measurements were repeated for each film for several top-bottom electrode geometry configurations.

Photo-pyroelectric response parameters

R is defined as the ratio of photo-pyroelectric current to the intensity of the incident light, i.e., $R = I_{\text{pyro}}/P \times S$ and D represents the ability to detect weak light signals that can be defined using the formula $D = R/(2eI_{\text{dark}}/S)^{0.5}$, where I_{pyro} , S , P , e , I_{dark} are the photo-pyroelectric current response, effective area of the device plane, intensity of the incident light, charge of an electron and dark current

Pyroelectric energy harvesting by Olsen cycle

The Olsen pyroelectric energy conversion cycle is fundamentally an electric form of a heat engine which allows repeatedly extracting electrical energy from the pyroelectric medium.^{11,14} However, it is required to cycle the temperature as well as the electrical condition of the pyroelectric material. Fig. 4b portrays the P - E diagram for AD₂A-film based pyroelectric device consists of two isotherms and two constant overlapping electric field lines.

Considering the shaded area bounded by A-B-C-D, which is the Olsen energy conversion cycle, AD₂A films provide energy density of 1.4 J L⁻¹ which is defined as follows:

$$N_D = \oint E dP$$

The corresponding power density P_D is the amount of energy generated by the pyroelectric material per unit volume per unit time which is calculated to be 0.093 W L^{-1} and defined as follows:

$$P_D = f N_D \text{ (where, } f \text{ is the overall cycle frequency)}$$

The corresponding scaled efficiency (η_{Olsen}) was calculated to be 0.25 % and defined as follows:

$$\eta / \eta_{\text{carnot}} = \left[\frac{T_{\text{high}}}{\Delta T} \frac{\oint E \cdot dP}{\int_{T_{\text{low}}}^{T_{\text{high}}} C(T) dT} \right]$$

where $\left(\frac{T_{\text{high}}}{\Delta T} \right)^{-1}$ is represented as Carnot efficiency, $\oint E \cdot dP$ is the total work done by the cycle and $\int_{T_{\text{low}}}^{T_{\text{high}}} C(T) dT$ is the total thermal energy input to the active device with a temperature-dependent heat capacity $C(T)$. It is assumed that $C(T)$ changes only with temperature and remains constant with electric field across the range under investigation.

References

- 1 P. Ueberschlag, *Sens. Rev.*, 2001, **21**, 118–126.
- 2 B. Ploss and A. Domig, *Ferroelectrics*, 1994, **159**, 263–268.
- 3 S. Bauer and S. B. Lang, *IEEE Trans. Dielectr. Electr. Insul.*, 1996, **3**, 647–676.
- 4 N. Neumann, R. Köhler and G. Hofmann, *Integr. Ferroelectr.*, 1995, **6**, 213–230.
- 5 A. Navid, C. S. Lynch and L. Pilon, *Smart Mater. Struct.*, 2010, **19**, 055006.
- 6 R. W. Whatmore and R. Watton, *Ferroelectrics*, 2000, **236**, 259–279.
- 7 M. Dietze, J. Krause, C.-H. Solterbeck and M. Es-Souni, *J. Appl. Phys.*, 2007, **101**, 054113.
- 8 A. W. Stephens, A. W. Levine, J. Fech, T. J. Zrebiec, A. V. Cafiero and A. M. Garofalo, *Thin Solid Films*, 1974, **24**, 361–379.

- 9 S. B. Lang, A. S. DeReggi, M. G. Broadhurst and G. Thomas Davis, *Ferroelectrics*, 1981, **33**, 119–125.
- 10 R. B. Olsen, D. A. Bruno, J. M. Briscoe and E. W. Jacobs, *J. Appl. Phys.*, 1985, **57**, 5036–5042.
- 11 A. Navid and L. Pilon, *Smart Mater. Struct.*, 2011, **20**, 025012.
- 12 M. Ikura, *Ferroelectrics*, 2002, **267**, 403–408.
- 13 L. Kouchachvili and M. Ikura, *J. Electrostat.*, 2007, **65**, 182–188.
- 14 H. Nguyen, A. Navid and L. Pilon, *Appl. Therm. Eng.*, 2010, **30**, 2127–2137.
- 15 H. Zhu, S. Pruvost, P. J. Cottinet and D. Guyomar, *Appl. Phys. Lett.*, 2011, **98**, 222901.
- 16 G. Cha and Y. S. Ju, *Sens. Actuators Phys.*, 2013, **189**, 100–107.
- 17 W. Li, G. Tang, G. Zhang, H. M. Jafri, J. Zhou, D. Liu, Y. Liu, J. Wang, K. Jin, Y. Hu, H. Gu, Z. Wang, J. Hong, H. Huang, L.-Q. Chen, S. Jiang and Q. Wang, *Sci. Adv.*, **7**, 3068.